Biosensors and Bioelectronics 142 (2019) 111514

Contents lists available at ScienceDirect

Biosensors and Bioelectronics

journal homepage: www.elsevier.com/locate/bios

Superstructure of silver crystals in a caged framework for plasmonic inverse sensing

Oole van de Donk[a,b,1], Xiaomin Zhang[a], Giuseppina Simone[a,1,*]

[a] The Ministry of Education Key Laboratory of Micro/Nano Systems for Aerospace, School of Mechanical Engineering, Northwestern Polytechnical University, 127 West Youyi Road, Xi'an, Shaanxi, 710072, People's Republic of China

[b] Department of Mechanical Engineering, Avans University of Applied Sciences, Lovensdijkstraat 61–63, Breda Noord-Brabant, 4818 AJ, Breda, the Netherlands

ARTICLE INFO

Keywords:
Inverse biosensing
SPR
Micro-pot reactor
GOx

ABSTRACT

Lowering the limit of detection is key to the design of sensors. Conventional transducers generate a signal proportional to the concentration of the molecule, but low concentrations are still difficult to detect with confidence.

Here we present an inverse sensor that induces a signal that is larger when the target molecule is less concentrated. Each sensor consists of a micro-pot reactor with an inner volume for storing the reactants and the cage walls, over which many silver hotspots are spread, working as optical antenna to produce amplification of the signal.

The aim is to attain inverse sensitivity during the enzymatic reaction, where reduction of the silver occurs.

We demonstrate the sensitivity and robustness of this approach by detecting glucose concentrations down to 10^{-12} M.

1. Introduction

Surface plasmon sensing is based on the fundamental principle of the interaction of polarized light with noble metals. Recently, it has been shown that the introduction of plasmonic nano-structures onto surface plasmon resonance (SPR) surfaces results in the introduction of local phenomenon, which provides a significant increase in sensitivity (Agrawal et al., 2018). The physical principle behind this improvement is given by the over-position of the local signals; the nano-structured surfaces and nano-particles, like an optical nanoscopic antenna, absorb and concentrate light energy into a very small volume, reducing the detection limit of SPR sensing to zeptomoles with a consequent enhancement of the sensitivity (De Angelis et al., 2008; McFarland and Van Duyne, 2003; Vance and Sandros, 2014). Besides, the light creates intense electric fields within a few nanometres of a nano-structured surface, which enhances the scattering of adsorbed molecules, providing a rich fingerprint spectrum containing all chemical information (Rodrigo et al., 2015; Subramanian et al., 2018). It has also been shown that coupling the nano-structured arrays to a surface or fibres in which Bragg diffraction gratings have been generated can extend the applications to multiplexed detection of several different analytes (Machida et al., 2018). In exploiting the antenna effect generated by the over-position of the electric fields around the nano-features, more complicated nano-probes can be designed and used in combination with the SPR to improve the spatial resolution and increment the signal-to-noise ratio (Schmidt et al., 2012; Liu and Huang, 2013). Moreover, the nano-structured surface in combination with SPR exhibits the main advantage of allowing detection of absorption, scattering, and fluorescence properties for biosensing (Li et al., 2018; Forato et al., 2019).

Nano-structured surfaces and nano-particles can be used to enhance the sensitivity as well as the tunability of the resonance. As observed above, the plasmonic phenomenon depends on the change of the refractive index of the nano-probes, which in turn is influenced by intrinsic parameters of the noble metal and by environmental parameters (Mayer and Hafner, 2011; Rodríguez-Lorenzo et al., 2009) (backbone and density of the surrounding or immobilized molecules, electron cavities) (Jeong et al., 2016; Simoncelli et al., 2018). Then, metal nanostructures such as crystals, particles, or stars are the starting point for the design of new biosensors.

Hybrid structures consisting of an organic framework in which metallic crystals are embedded are promising candidates for a variety of applications including gas storage/separation, catalysis as well as optical sensing. They provide a large void space that can accommodate other active species for promoting a red-shift to the near-infrared region

* Corresponding author.
E-mail address: giuseppina.simone@nwou.edu.cn (G. Simone).
[1] Authors with equal contribution.

https://doi.org/10.1016/j.bios.2019.111514
Received 25 April 2019; Received in revised form 15 June 2019; Accepted 13 July 2019
Available online 13 July 2019
0956-5663/

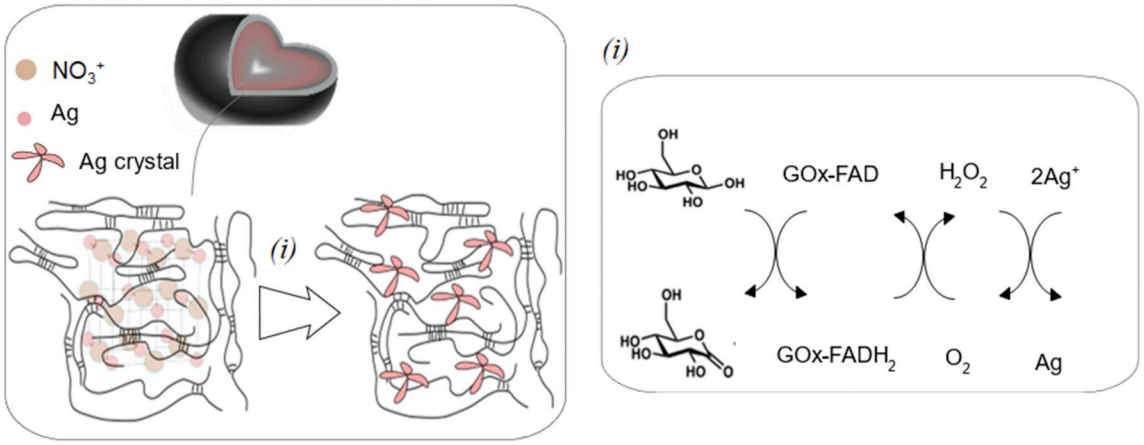

Fig. 1. Mechanism of production of the cage. Left: The cross-section of the cage is schematized on top. The grey thickness represents the proteinaceous shell. The inner part of the shell shows the inner volume and it is represented by a gradient of colours (from pink to white) with the aim to reproduce a 3D sketch. The shell is made of a proteinaceous framework including Ag salt cubic crystals ($AgNO_3$). After reaction (i) of the reduction of the glucose via GOx, the H_2O_2 produced the Ag^0 (pink stars gelatin matrix on the right of the arrow). Right: The detailed scheme of the reaction is represented. (For interpretation of the references to colour in this figure legend, the reader is referred to the Web version of this article.)

(Aubry et al., 2010).

In this context, we aimed to develop highly sensitive nano-probes for the measurement of surface plasmon resonance. These probes consist of a porous shell decorated by countless hotspots and permitting the sample to enter and be stored into the inner volume.

We evolved this concept by generating silver nanostructures by growing silver crystals *in situ* while detecting the reduction reactions into the micro-pot reactor (Sun and Li, 2018; Wang et al., 2018; Zhang and Simone, 2019). Then, in our approach, the plasmonic resonance is tuned by programming crystal growth to favour the formation of a transducer around the organic framework (Schwartzberg et al., 2006).

It has already been shown that enzymes can react to generate nanostructures of controlled size by limiting the rate of nucleation (De la Rica and Matsui, 2008; Kisailus et al., 2006). Glucose oxidase was shown to affect the rate of crystallization, permitting the design of nucleation or growth of nanocrystals to tailor the plasmonic behaviour of silver sensors (Rodríguez-Lorenzo et al., 2012).

Here a proteinaceous caged framework whose network includes silver nitrate ($AgNO_3$) has been fabricated with the aim of enhancing plasmonic sensitivity. Fig. 1 shows the scheme of the work. The shell cages consisted of a protein framework including silver. The cages include countless silver spots which contribute to enhancing the sensitivity.

For the analysis, the plasmonic microreactors were filled with glucose oxidase and then exposed to the substrate, glucose. The mechanism of the reaction schematized in panel *(i)* of the figure was triggered and the silver was reduced by the hydrogen peroxide generated during the reactions of the ions embedded in the matrix.

The reduction of the silver shifts the plasmonic signal according to the concentration of the substrate and the duration of the reaction.

Each shell particle in the ensemble potentially serves as an independent sensor, which is promising in applications for measurements in solution or inside cells and tissues, where fixed arrays are unable to penetrate.

2. Experimental section

2.1. Materials

Gelatin (type A, Bloom 300, dynamic viscosity: 1.5–6.0 mPa), glutaraldehyde (50% v/v), Span 83, mineral oil, acetone, ethanol, (3-mercaptopropyl)trimethoxysilane, and $AgNO_3$ were from Sigma Aldrich, China, and were used as received. Gelatin was used without further purification and prepared as 15 wt%. Milli-Q-grade water was used as solvent. GOx and glucose were also received from Sigma Aldrich, China.

2.2. SPR setup

The study was done using a homemade SPR system. The light beam from a laser (650-nm red dot laser, 5 mW, Shenzhen Fuzhe Technology Co., Ltd.) was tuned by variable resistance in the power supply (2-kOhm resistance, 3590S-2-202 L, Bourns, Inc.). The light was p-polarized by a double Glan-Taylor Calcite Polarizer (Thorlabs Inc.) and then centred by a microbench alignment plate with a 1-mm hole (Qioptic, G061680000) before it reached the prism. After internal reflection in the prism, the light was polarized by a second polarizer (Thorlabs, Glan Thomson polarizer BBAR: 650–1050 nm, CA: 10.0 mm). The light was caught by a reflective collimator (Thorlabs Inc. RC12FC-P01) and measured by an Ocean Optics HR4000 (custom) spectrometer. The laser, the first polarizer, and the alignment plate were mounted on a high-precision polarizer mount (Standa, 5PPH50-1). By turning the polarizer mount, the angle of reflection in the prism changed. The second polarizer and collimator were mounted on a second and similar polarizer mount. The angle was determined by sourcing the highest light intensity. SpectraSuite software plotted the light intensity of the reflected light against the wavelength (0–1050 nm).

2.3. Particle preparation by droplet generation

The cages were prepared as follows: a mixture of mineral oil (5 mL), glutaraldehyde (2 mL, 50% v/v), and deionized water (20 mL) was prepared in the presence of Span 83 (50 µL). Span 83 was selected as a surfactant to emulsify the aqueous and oil phases in the selected amounts.

After stirring at 1000 rpm for 1 h at room temperature, the emulsification was completed by ultrasonicating the mixture for 240 s at 90% amplitude under ice cooling. An aqueous solution of the protein (15 wt %) was prepared by mixing the protein in Millipore water at 40 °C for 1 h. Then, 5% v:v of 0.1 M $AgNO_3$ solution was added. Next, the gelatin and the microemulsion were pumped inside the microfluidic chip. The microchip and the setup have been widely described elsewhere (Zhang and Simone, 2019; Simone, 2015; Pepe et al., 2017).

To test the sensitivity of the cages, they were immobilized on top of a glass slide coated with (3-mercaptopropyl)trimethoxysilane deposited by vapour (Simone et al., 2010).

Next, they were incubated overnight with a solution of 1 unit/mL of GOx to permit the diffusion and absorption of the enzyme into the inner cavity. Different concentrations of glucose were then tested.

2.4. Characterization

The morphology and structure of the prepared particles were evaluated by Tescan Vega3 scanning electron microscope (Laboratory of Mechanical Engineering, Northwestern Polytechnical University, Xi'an, China) at 16 kV (extra-high tension). Samples for scanning electron microscopy (SEM) were prepared by dropping purified capsule dispersions on silicon wafers that were then dried at room temperature. For the investigations, the samples were sputtered with gold for 2 min. The morphology, elemental composition, and housing of the Ag particles inside the molecular structure of the gelatin were analysed by transmission electron microscope (Hitachi H-7650) at 200 kV with outstanding high-resolution transmission electron microscope (TEM) (Xi'a Jiangton University, Department of Life Science). Energy-dispersive X-ray spectroscopy EDS analysis was carried on. The samples were embedded in resin and ultramicrotomy was carried out at room temperature. The X-ray diffractometer was used for the crystallographic analysis (Bruker D8 Discover, Shaanxi Materials Analysis and Research Center. School of Materials Science and Engineering, Northwestern Polytechnical University) and the raw data analysed by X'Pert High Score and the results were analysed by FullPro-Suite software.

3. Results and discussion

3.1. Design and synthesis

The scheme of preparation of the shell particles including the Ag nitrate is shown in Fig. 2 (left). The precursor of the particles consisted of a mixture of the proteinaceous molecules and $AgNO_3$, which was injected inside a fluidic microchannel for the generation of droplets. The procedure for the typical production of the cages has already been explained (Zhang and Simone, 2019). The mixture and oil were pumped inside the microfluidic T-shaped channel and a third side channel was used to pump an emulsion including the crosslinker. In contact with the droplets, the emulsion including the glutaraldehyde crosslinked the protein cages (Simone, 2015; Pepe et al., 2017). The aqueous glutaraldehyde and oil mixed with the surfactant, generating a nano-emulsion which controlled the mechanism of the crosslinker diffusion across the thickness of the droplets. The aqueous solution of crosslinker and oil formed micelles, owing to the hydrophobic interaction between the oil and the alkyl chains of the surfactant. This one-vessel and *sans-template* protocol allowed collection of the spheroidal proteinaceous cages, which were shown to have a controllable aspect ratio (Fig. 2, right) (Zhang and Simone, 2019).

SEM images of the spheroidal cage revealed countless crystals of silver tiling on the surface of the shell (Fig. 3a). The $AgNO_3$ coating the shell was uniform (Fig. 3b), and the elemental composition, as determined by energy-dispersive X-ray spectroscopy and expressed in mass fractions, was 4.3% Ag, 40.5% C, 15.5% O, and 30.2% F (Fig. 3c). The fluorine was a residual of the carrier oil used for the preparation of the cages. To assess the ability of the cages to shield the internal cavities and allocate the metal nitrate into the cage walls, an investigation of the Ag entangled in the proteinaceous caged framework was carried out by TEM, after ultramicrotomy of the sample. This made it possible to compare the surface analysis provided by the SEM with the bulk properties. The transmission electron micrographs in Fig. 3d represents the sample observed at high resolution. The crystals (black dots) in the form of single structures decorated the proteinaceous matrix in correspondence of thin thickness of the framework. An overview of the bulk crystals of silver confirmed that they were constructed in the network and had a median size equal to 1.4 nm (Fig. 3e). The analysis also evidenced the presence of porosity available to host the silver during the process of cage formation and to provide a 3D network (the white spot in the matrix) for templating the crystal growth during the following steps (De Angelis et al., 2010). The elemental composition extant in the network was measured as containing 0.17 wt% Ag (Fig. 3f) and the crystallographic configuration of the silver nitrate tiling the surface of the polymeric framework showed the characteristic diffractometric peaks at $2\theta = 29.87^\circ$ for the {-10-1} crystal plane, $2\theta = 41.90^\circ$ for the {00-2} crystal plane, $2\theta = 52.31^\circ$ for the {-200} crystal plane, and finally $2\theta = 73.03^\circ$ for the {2-10} crystal plane. (Fig. 3g).

3.2. Plasmonic sensing

The sensitivity was examined in a homemade surface plasmon resonance spectrometer under red-light illumination (Fig. 4a), where the reflected light was spectrally resolved with an optical sensor.

Before testing the behaviour as a plasmonic sensor, the reflectance of the cage with the light incidence angle was measured for detecting the maximum of the absorbance (Fig. 4b); the resonance was observed at an angle of 64.67°. The spectrum intensity of the reflected light was fitted to a Lorentz function, which could be used to extract the full width at half maximum (FWHM, 4.85 ± 0.03 nm) (Fig. 4c).

Then, the cages were used as reactors to track the enzymatic reaction between the GOx and the glucose. They were filled with the two solutions of glucose (several concentrations) and GOx by the mechanisms of both diffusion through the porous framework and absorption (Zhang and Simone, 2019). As an advantage, each cage could work as an independent micro-reactor with its walls coated by countless silver spots enhancing the plasmonic signal. The cages were positioned under the plasmonic setup (Schasfoort, 2017a) to be used as a plasmonic transducer of GOx activity when the Ag localizes the low-energy plasmon mode, which results in a dominant SPR band, as observed in Fig. 4b. After activating the enzymatic reaction, the production of hydrogen peroxide began according to the scheme reproduced in Fig. 1.

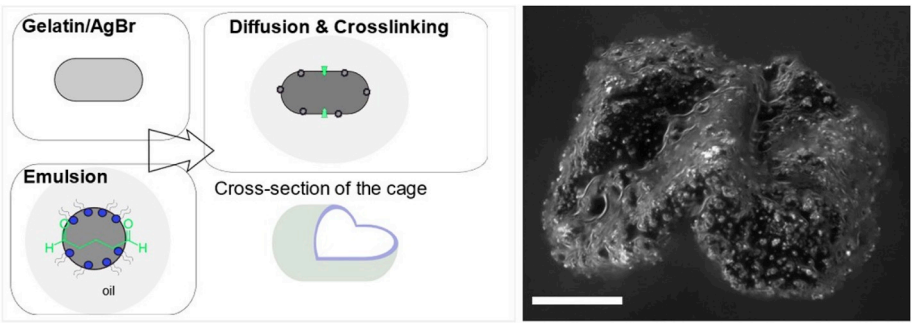

Fig. 2. Left: Description of the fabrication process. The green arrows show the direction of diffusion. Right: Cage with the Ag crystals. Scale bar: 70 µm. (For interpretation of the references to colour in this figure legend, the reader is referred to the Web version of this article.)

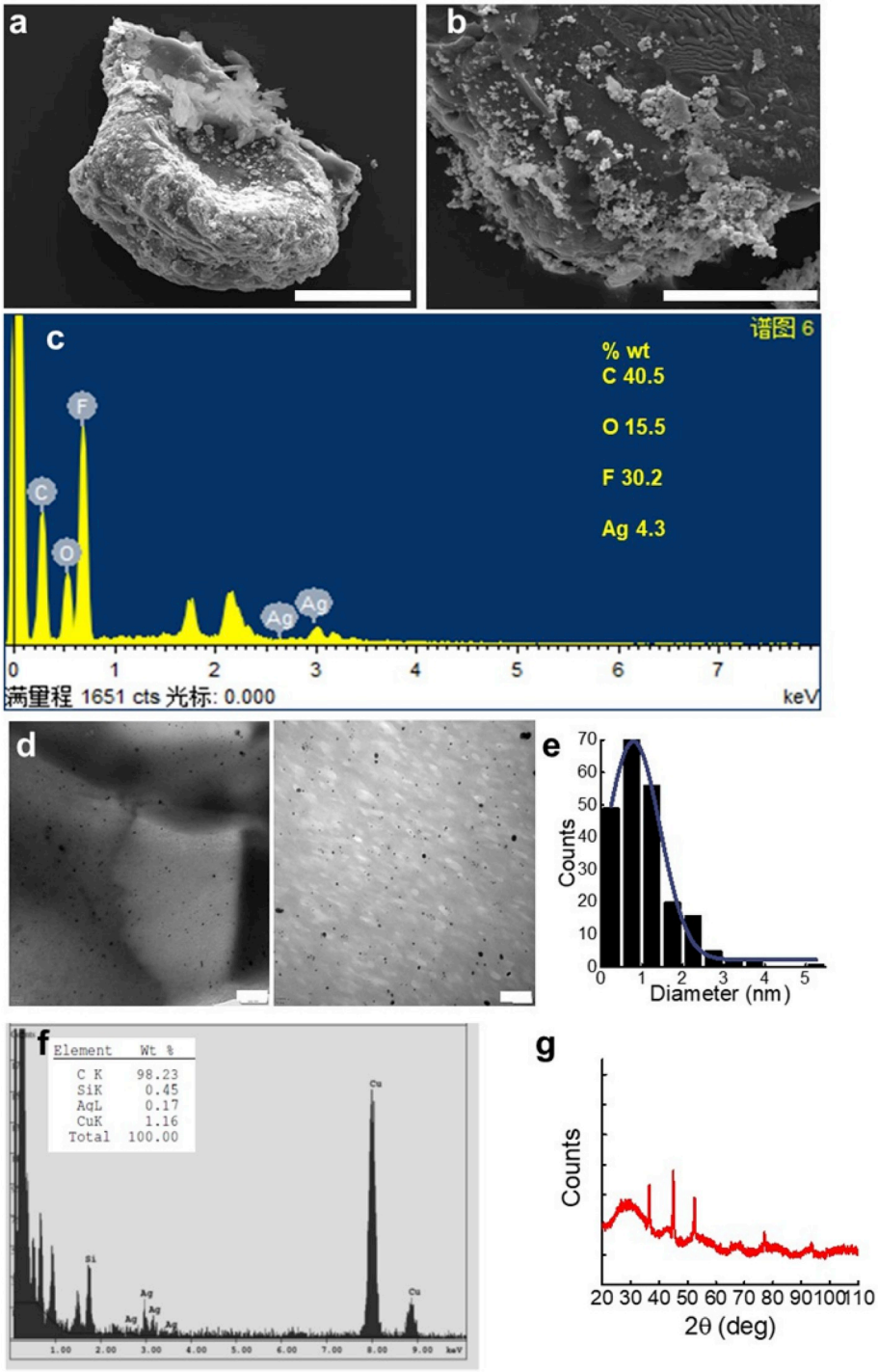

Fig. 3. (a) SEM micrograph of the cages. Scale bar: 40 µm. **(b)** High-resolution SEM image of the cage with details of the Ag-crystal coating. Scale bar: 20 µm. **(c)** EDS spectrum of Ag nanoparticles housed in a gelatin network. **(d)** TEM image of Ag crystals (black dots) entangled in the ultramicrotomy proteinaceous framework. Scale bar: left 500 nm (magnification 3000×), right 100 nm (magnification 10000×). **(e)** Diameter distribution of the Ag crystals and cumulative distribution. **(f)** EDS spectrum of Ag housed in a gelatin network. **(g)** X-ray diffraction diagram of the cage after preparation. $AgNO_3$ characteristic diffractometric peaks at $2\theta = 29.87^{\circ}$ for the {-10-1} crystal plane, $2\theta = 41.90^{\circ}$ for the {00-2} crystal plane, $2\theta = 52.31^{\circ}$ for the {-200} crystal plane, and finally $2\theta = 73.03^{\circ}$ for the {2-10} crystal plane.

The H_2O_2 reacted with the silver nitrate, reducing the silver from the Ag^+ state to Ag^0. Upon the reduction, there was a shift of the absorbance to lower wavelengths (Fig. 5a). The shift in presence of the reduction of the silver has been extensively studied, showing that the time evolution of UV-visible-NIR extinction spectra during the reduction results in the principal band blue-shifting (Fernanda Cardinal et al., 2010). During our experiments, the rate of the reaction was slow at the beginning (the curves almost overlap), when an irrelevant shift of the peak was observed, but after 2 min, the rate increased; then, after 40 min, the silver was completely reduced.

The shift of the plasmonic band position as a function of glucose concentration is shown in Fig. 5b. The curve of absorbance shifted towards lower values when the concentration of glucose increased in the range between 10^{-12} and 10^{-6} M, displaying that in this range the quantity of the reduced silver raises. Higher concentrations of the substrate did not result in a further shift of the absorbance band, because of the saturation of the system. Besides, the wavelength decreased with a linear trend ($R^2 = 0.993$) until the concentration was lower than 10^{-4} M, and from that value the shift of the peak was negligible (Fig. 5c). Furthermore, the evaluation of $\Delta\lambda_{max}$ showed that the shift increases of 1.2 nm when the concentration of GOx decreases from 10^{-12} to 10^{-9} M and of 0.3 nm when the concentration of GOx decreases from 10^{-3} to 10^{-2} M.

The dynamics observed at the low and high concentrations of the

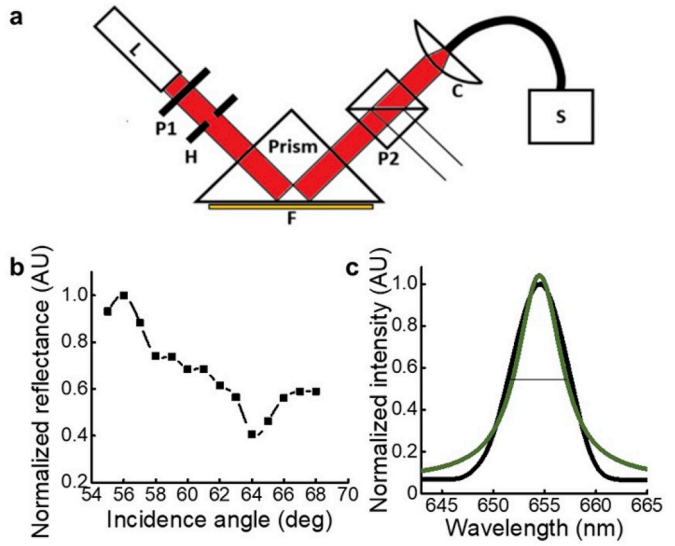

Fig. 4. (a) Homemade surface plasmon resonance spectrometer. C collimator; P1 and P2: polarizer; H: optical pinhole; L: laser at 650 nm; S: optical sensor; F: sample. **(b)** Reflectivity of cages in air according to the incidence angle. **(c)** Intensity of cages in air according to the wavelength. The lighter curve shows the Lorentz model used for the fitting ($R^2 = 0.99$). the normalization is defined as the ratio between the actual value recorded at the given angle or wavelength versus the maximum value.

substrate depends on the reaction with the enzyme, which in presence of the silver influences the rate of crystallization to favour either the nucleation or the growth of the nanocrystals (Jana et al., 2001). The rate of crystallization of the silver is strictly related to the rate of production of the H_2O_2 during the reaction between the enzyme and the substrate (Levenspiel, 1999; Callister and Rethwisch, 2007). Low concentrations of the reducing agent or of the substrate trigger slow crystal growth conditions and formation of a homogeneous silver coating, which yields a blueshift of the spectrum and a consequent higher sensitivityLee et al., 2018). At high concentrations of one of the reactants, free-standing silver nanocrystals are obtained with a smaller variation of the optical properties of the plasmonic transducers by means of the formation of a silver coating.

Upon analyzing the trend of the signal according to time of the reaction (Fig. 5d), it emerged that at concentrations lower than 10^{-3} M, the sensorgram clearly transduced and tracked the steps of the process. First, the adsorption on the surface of the molecules after the injection, resulting in a change of the refractive index, then a shift of the SPR angle, relative to the association, and finally the decay of the signal given by the injection of the new sample were shown (Hulme and Trevethick, 2010). Hence, in correspondence with the highest concentrations (10^{-3} M and 10^{-2} M), the signal was unclear, the reaction did not take place, and the trend of intensity according to time just showed the peak related to the difference in refractive indices due to the presence of the sample, named the bulk effect (Schasfoort, 2017b).

This system producing an inverse relationship between concentration and signal belongs to the class of the inverse sensitivity biosensors and is suitable for designing and producing ultrasensitive sensors for biological applications because of the ability to differentiate low intensity signals from the zero-signal obtained in the absence of the target molecule.

However, all this seems to highlight an important criticism of this method, because the system is applicable for enzyme-based sensors but not suitable for different assays. It has been already suggested that for generalizing the use, the GOx can be bound to antibodies and used as the label in a classical enzyme-linked immunoassay with a sensitivity down to single molecule (Nehl et al., 2006); where the only disadvantage is due to the steps of preparation of the sample. Our system

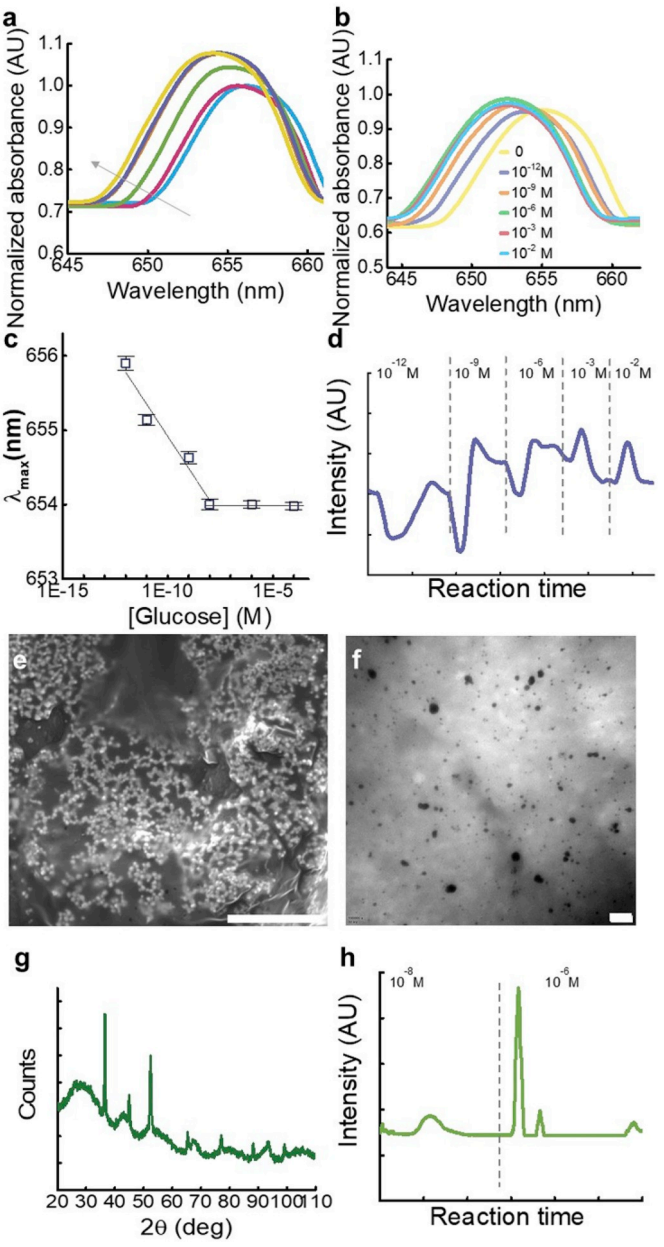

Fig. 5. (a) Normalized absorbance (defined as the actual absorbance versus the maximum absorbance) versus the wavelength according to the time, growing into the direction of the arrow. The reduction of silver from the Ag^+ state to Ag^0 as tracked by the SPR sensor, showing the shift of the absorbance to lower wavelength. **(b)** Normalized absorbance (defined as the actual absorbance versus the maximum absorbance) versus the wavelength according to the glucose concentration. Independent experiments with different glucose concentrations were carried on after the cage regeneration. The shift of the plasmonic band position as a function of glucose showed that the curve of absorbance shifted towards lower values when the concentration of glucose increased in the range between 10^{-12} and 10^{-6} M. **(c)** λ_{max} versus concentration of glucose. The values represent the mean ± SD of three individual experiments (reproducibility of the data 95%). The range of concentration between 10^{-12} and 10^{-9} M is linearly fitted ($R^2 = 0.99$); at higher concentrations, λ_{max} is independent. **(d)** Signal intensity according to reaction time, measured at 63.4°. The dashed lines delimit the range of time for each concentration. 10^{-3} and 10^{-2} M did not show the characteristic trend of reaction. **(e)** SEM image obtained after silver reduction in the presence of enzyme, evidencing free-standing quasi-spherical nanoparticles coating the surface and the inside of the proteinaceous network. Scale bar: 20 μm. **(f)** TEM image of cage nanoparticles entangled in the framework. Scale bar: 100 nm. **(g)** X-ray diffraction diagram of the cage after preparation. at 2θ = 44.89° for the {-1-1-1} crystal plane, 2θ = 52.31° for the {-200} crystal plane, and finally at 2θ = 77.13° for the {-2-20} crystal plane. **(h)** Signal intensity according to reaction time. The dashed line delimits the range of time for each concentration of the globular protein.

exploits the advantages of independent miniaturized reactor where to run and track the reaction and permits to reduce the steps of sampling and consequently the losses as well as the uncertainty of the measurements. Besides, several important cellular pathways produce the H_2O_2 and the inverse sensitivity can support the transduction and tracking of those signals (Zhang et al., 2013).

Then the reduction to Ag^0, the sensors were analysed, and Fig. 5e and f shows the SEM and TEM results. They were observed following the enzymatic incubation with 10^{-9} M glucose. The representative SEM images obtained after silver reduction in the presence of enzyme evidenced free-standing quasi-spherical nanoparticles coating the surface and inner volume of the proteinaceous network. The quasi-spherical shape of the crystal is provided by the rate of reaction to favour the nucleation more than the crystallization, as explained above.

The X-ray diffractometric analysis demonstrated that after oxidization, the Ag had the characteristic diffractometric peaks of the crystal plane at $2\theta = 44.89^\circ$ for the {-1-1-1} crystal plane, $2\theta = 52.31^\circ$ for the {-200} crystal plane, and finally $2\theta = 77.13^\circ$ for the {-2-20} crystal plane (Fig. 5g).

Next, an experiment to prove the robustness and specificity of plasmonic sensors was designed. First the cages were regenerated by incubation with the fresh GOx, which, according to the reaction in Fig. 1, allowed the oxidation of the Ag. Then, the sensor activity was tested using bovine serum albumin diluted to different concentrations in phosphate saline buffer. Two concentrations of the non-specific globular protein were tested, 10^{-8} and 10^{-6} M. The course of the intensity of the reaction during the tracking time (Fig. 5h) did not show a consistent trend of the reaction. The sensorgram only showed the peaks in correspondence of the sample uploading, highlighting the feeding of the protein, the adsorption or the interaction with the substrate. All this was translated into a change of the recorded intensity as an artefact or the bulk effect (Zhang et al., 2013).

4. Conclusion

In conclusion, the present study introduced Ag^+ ions in a proteinaceous caged framework as hotspots for plasmonic sensing. Silver ions in the form of nitrate were introduced in the liquid solution of the protein before the droplet-based fabrication. An in-depth analysis showed the presence of $AgNO_3$ crystals in the network and tiling on the surface of the crosslinked framework. Each cage had the advantage of working as an individual reactor with countless spots providing enhanced sensitivity, where the inner volume of the cage stores the reactants. Besides, the micro-pots can be used several times with different compounds as they are label-free.

Inverse sensitivity of the silver ions was shown for the enzymatic reaction of the glucose substrate via GOx and the plasmonic behaviour of the system was analysed.

The reduction of the silver from the Ag^+ state to Ag^0 as tracked by the SPR sensor showed a shift of the absorbance to lower wavelength. A shift of the plasmonic band position was also observed as a function of glucose concentration. Besides, it was shown that the curve of absorbance shifted towards lower values when the concentration of glucose increased in the range between 10^{-12} and 10^{-6} M, with a significant shift of λ_{max}, but above that concentration limit, the measured shift was small. The course of the signal intensity according to reaction time confirmed that above certain values of glucose concentration, the reaction cannot take place. Following the silver reduction, the analysis evidenced free-standing quasi-spherical nanoparticles coating the surface and inside of the proteinaceous network. Besides, the crystallographic configuration showed the characteristic peaks of the silver plane.

In conclusion, we designed a control experiment where the activity of a globular non-specific protein was tested. Under this experimental condition, the course of the signal did not show significant changes and no shift of the peak was observed.

The results indicate numerous capabilities of the inverse sensors for tracking biochemical enzymatic reactions where tiny amounts of molecules are available. Finally, the localized plasmon resonance used to realize a signal-generation mechanism that is inversely proportional to concentration will boost the development in sensing.

Declaration of competing interest

The authors declare that they have no known competing financial interests or personal relationships that could have appeared to influence the work reported in this paper.

Acknowledgments

This work was supported by the Fundamental Research Funds for the Central Universities (G2016KY0302). G.S. acknowledges the support from the Northwestern Polytechnical University for the visiting scholarship.Besides, the authors thank Dr. Guo Yao for her support with the XRDtest and analysis of the data and Dr.P. Podesva for the help with thepicture in Fig. 2.

References

Agrawal, A., Cho, S.H., Zandi, O., Ghosh, S., Johns, R.W., Milliron, D.J., 2018 Feb 5. Localized surface plasmon resonance in semiconductor nanocrystals. Chem. Rev. 118 (6), 3121–3207.

Aubry, A., Lei, D.Y., Fernández-Domínguez, A.I., Sonnefraud, Y., Maier, S.A., Pendry, J.B., 2010 Jun 2. Plasmonic light-harvesting devices over the whole visible spectrum. Nano Lett. 10 (7), 2574–2579.

Callister, W.D., Rethwisch, D.G., 2007. Materials Science and Engineering: an Introduction. John Wiley & Sons, New York.

De Angelis, F., Patrini, M., Das, G., Maksymov, I., Galli, M., Businaro, L., Andreani, L.C., Di Fabrizio, E., 2008 Jul 17. A hybrid plasmonic− photonic nanodevice for label-free detection of a few molecules. Nano Lett. 8 (8), 2321–2327.

De Angelis, F., Das, G., Candeloro, P., Patrini, M., Galli, M., Bek, A., Lazzarino, M., Maksymov, I., Liberale, C., Andreani, L.C., Di Fabrizio, E., 2010 Jan. Nanoscale chemical mapping using three-dimensional adiabatic compression of surface plasmon polaritons. Nat. Nanotechnol. 5 (1), 67.

De la Rica, R., Matsui, H., 2008. Urease as a nanoreactor for growing crystalline ZnO nanoshells at room temperature. Angew. Chem. Int. Ed. 47, 5415–5417.

Fernanda Cardinal, M., Rodríguez-González, B., Alvarez-Puebla, R.A., Pérez-Juste, J., Liz-Marzán, L.M., 2010 May 18. Modulation of localized surface plasmons and SERS response in gold dumbbells through silver coating. J. Phys. Chem. C 114 (23), 10417–10423.

Forato, F., Talebzadeh, S., Rousseau, N., Mévellec, J.Y., Bujoli, B., Knight, D.A., Queffelec, C., Humbert, B., 2019. Functionalized core-shell Ag@ TiO2 nanoparticles for enhanced Raman spectroscopy: a sensitive detection method for Cu (II) ions. Phys. Chem. Chem. Phys. 21 (6), 3066–3072.

Hulme, E.C., Trevethick, M.A., 2010 Nov. Ligand binding assays at equilibrium: validation and interpretation. Br. J. Pharmacol. 161 (6), 1219–1237.

Jana, N.R., Gearheart, L., Murphy, C.J., 2001. Evidence for seed-mediated nucleation in the chemical reduction of gold salts to gold nanoparticles. Chem. Mater. 13, 2313–2322.

Jeong, H.H., Mark, A.G., Alarcón-Correa, M., Kim, I., Oswald, P., Lee, T.C., Fischer, P., 2016 Apr 19. Dispersion and shape engineered plasmonic nanosensors. Nat. Commun. 7, 11331.

Kisailus, D., Schwenzer, B., Gomm, J., Weaver, J.C., Morse, D.E., 2006. Kinetically controlled catalytic formation of zinc oxide thin films at low temperature. J. Am. Chem. Soc. 128, 1027610280.

Lee, K.L., Chang, C.C., You, M.L., Pan, M.Y., Wei, P.K., 2018 Jun 27. Enhancing surface sensing sensitivity of metallic nanostructures using blue-shifted surface plasmon mode and fano resonance. Sci. Rep. 8 (1), 9762.

Levenspiel, O., 1999 Nov 1. Chemical reaction engineering. Ind. Eng. Chem. Res. 38 (11), 4140–4143.

Li, G., Chen, Y., Zhang, L., Zhang, M., Li, S., Li, L., Wang, T., Wang, C., 2018 Mar 1. Facile approach to synthesize gold nanorod@ polyacrylic acid/calcium phosphate yolk-shell nanoparticles for dual-mode imaging and pH/NIR-responsive drug delivery. Nano-Micro Lett. 10 (1), 7.

Liu, Y., Huang, C.Z., 2013. Screening sensitive nanosensors via the investigation of shape-dependent localized surface plasmon resonance of single Ag nanoparticles. Nanoscale 5 (16), 7458–7466.

Machida, M., Nakajima, Y., Torres-Mapa, M.L., Heinemann, D., Heisterkamp, A., Terakawa, M., 2018 Jan 9. Shrinkable silver diffraction grating fabricated inside a hydrogel using 522-nm femtosecond laser. Sci. Rep. 8 (1), 187.

Mayer, K.M., Hafner, J.H., 2011 Jun 8. Localized surface plasmon resonance sensors. Chem. Rev. 111 (6), 3828–3857.

McFarland, A.D., Van Duyne, R.P., 2003 Aug 13. Single silver nanoparticles as real-time optical sensors with zeptomole sensitivity. Nano Lett. 3 (8), 1057–1062.

Nehl, C.L., Liao, H., Hafner, J.H., 2006 Apr 12. Optical properties of star-shaped gold

nanoparticles. Nano Lett. 6 (4), 683–688.
Pepe, A., Podesva, P., Simone, G., 2017 Jul 20. Tunable uptake/release mechanism of protein microgel particles in biomimicking environment. Sci. Rep. 7 (1), 6014.
Rodrigo, D., Limaj, O., Janner, D., Etezadi, D., De Abajo, F.J., Pruneri, V., Altug, H., 2015 Jul 10. Mid-infrared plasmonic biosensing with graphene. Science 349 (6244), 165–168.
Rodríguez-Lorenzo, L., Alvarez-Puebla, R.A., Pastoriza-Santos, I., Mazzucco, S., Stéphan, O., Kociak, M., Liz-Marzán, L.M., García de Abajo, F.J., 2009 Mar 17. Zeptomol detection through controlled ultrasensitive surface-enhanced Raman scattering. J. Am. Chem. Soc. 131 (13), 4616–4618.
Rodríguez-Lorenzo, L., de La Rica, R., Álvarez-Puebla, R.A., Liz-Marzán, L.M., Stevens, M.M., 2012 Jul. Plasmonic nanosensors with inverse sensitivity by means of enzyme-guided crystal growth. Nat. Mater. 11 (7), 604.
Schasfoort, R.B. (Ed.), 2017 May 30. Handbook of Surface Plasmon Resonance. Royal Society of Chemistry.
Schasfoort, R.B. (Ed.), 2017 May 30. Handbook of Surface Plasmon Resonance. Royal Society of Chemistry.
Schmidt, M.A., Lei, D.Y., Wondraczek, L., Nazabal, V., Maier, S.A., 2012 Oct 9. Hybrid nanoparticle-microcavity-based plasmonic nanosensors with improved detection resolution and extended remote-sensing ability. Nat. Commun. 3, 1108.
Schwartzberg, A.M., Oshiro, T.Y., Zhang, J.Z., Huser, T., Talley, C.E., 2006 Jul 1. Improving nano-probes using surface-enhanced Raman scattering from 30-nm hollow gold particles. Anal. Chem. 78 (13), 4732–4736.
Simoncelli, S., Li, Y., Cortés, E., Maier, S.A., 2018 Jan 18. Nanoscale control of molecular self-assembly induced by plasmonic hot-electron dynamics. ACS Nano 12 (3), 2184–2192.
Simone, G., 2015. Demonstrating microdroplet coalescence for tailored and biodegradable microgel fabrication. RSC Adv. 5 (70), 56848–56854.
Simone, G., Perozziello, G., Sardella, G., Disegna, I., Tori, S., Manaresi, N., Medoro, G., 2010 Jul 1. A microvalve for hybrid microfluidic systems. Microsyst. Technol. 16 (7), 1269–1276.
Subramanian, S., Wu, H.Y., Constant, T., Xavier, J., Vollmer, F., 2018 Dec. Label-free optical single-molecule micro-and nanosensors. Adv. Mater. 30 (51), 1801246.
Sun, Y., Li, T., 2018 Sep 3. Composition-tunable hollow Au/Ag SERS nano-probes coupled with target-catalyzed hairpin assembly for triple-amplification detection of miRNA. Anal. Chem. 90 (19), 11614–11621.
Vance, S.A., Sandros, M.G., 2014 May 30. Zeptomole detection of C-reactive protein in serum by a nanoparticle amplified surface plasmon resonance imaging aptasensor. Sci. Rep. 4, 5129.
Wang, Y., Zhao, P., Mao, L., Hou, Y., Li, D., 2018. Determination of brain injury biomarkers by surface-enhanced Raman scattering using hollow gold nanospheres. RSC Adv. 8 (6), 3143–3150.
Zhang, X., Simone, G., 2019 Jan 15. Gelatin cages: the formation and characterization of carriers for housing catalyst cargoes. Chem. Eng. J. 356, 516–523.
Zhang, Y., Choksi, S., Chen, K., Pobezinskaya, Y., Linnoila, I., Liu, Z.G., 2013 Jul. ROS play a critical role in the differentiation of alternatively activated macrophages and the occurrence of tumor-associated macrophages. Cell Res. 23 (7), 898.